Reflective and Transparent Cellulose-Based Passive Radiative Coolers

Sampath Gamage
Linköping University: Linkopings universitet
Md. Mehebub Alam
Linkopings universitet
Tomas Hallberg
FOI Sweden
Chriatina Akerlind
FOI, Sweden
Ayesha Sultana
Linkopings universitet
Magnus Berggren
Linkopings universitet
Xavier Crispin
Linkopings universitet
Hans Kariis
FOI, Sweden
Dan Zhao
Linkopings universitet
Magnus Jonsson (magnus.jonsson@liu.se)
Linköping University: Linkopings universitet https://orcid.org/0000-0002-3002-3639

Research Article

Keywords: Daytime passive radiative cooling, Nanocellulose, Reflective coolers, Transparent 22 coolers, Atmospheric transmittance, Radiative cooling materials

Posted Date: March 23rd, 2021

DOI: https://doi.org/10.21203/rs.3.rs-314524/v1

Version of Record: A version of this preprint was published at Cellulose on August 7th, 2021. See the published version at https://doi.org/10.1007/s10570-021-04112-1.

Reflective and transparent cellulose-based passive radiative coolers

Sampath Gamage[1,2], Md. Mehebub Alam[1], Tomas Hallberg[3], Christina Åkerlind[3], Ayesha Sultana[1,2], Magnus Berggren[1,2], Xavier Crispin[1,2], Hans Kariis[3], Dan Zhao[1], and Magnus P. Jonsson[1,2,*]

[1]Laboratory of Organic Electronics, Department of Science and Technology, Linköping University, SE-601 74 Norrköping, Sweden

[2]Wallenberg Wood Science Center, Linköping University, SE-601 74 Norrköping, Sweden

[3]FOI-Swedish Defense Research Agency, Department of Electro-Optical systems, 581 11 Linköping, Sweden

*Email: magnus.jonsson@liu.se

Abstract

Radiative cooling passively removes heat from objects via emission of thermal radiation to cold space. Suitable radiative cooling materials absorb infrared light while they avoid solar heating by either reflecting or transmitting solar radiation, depending on the application. Here, we demonstrate a reflective radiative cooler and a transparent radiative cooler solely based on cellulose derivatives manufactured via electrospinning and casting, respectively. By modifying the microstructure of cellulose materials, we can control the solar light interaction from highly reflective (>90%, porous structure) to highly transparent (≈90%, homogenous structure). Both cellulose materials show strong thermal emissivity and minimal solar absorption, making them suitable for daytime radiative cooling. Used as coatings on silicon samples exposed to sun light at daytime, the reflective and transparent cellulose coolers could passively reduce sample temperatures by up to 32 °C and 15 °C, respectively.

Keywords Daytime passive radiative cooling · Nanocellulose · Reflective coolers · Transparent coolers · Atmospheric transmittance · Radiative cooling materials

Introduction

Passive radiative cooling has the potential to reduce the world's energy-consumption by complementing and replacing traditional active methods to control indoor temperature, such as using air-conditioning. In contrast to traditional methods, radiative cooling requires no external energy to function. Instead, it utilizes the temperature difference between the cold outer space and the earth to passively radiate heat through the atmosphere, which conveniently has a transparency window in the infrared (IR) region that matches thermal radiation at room temperature. The net cooling power, P_{net} of a radiative cooler is given by:

$$P_{net} = P_{\mathrm{rad}} - P_{\mathrm{atm}} - P_{\mathrm{nonrad}} - P_{\mathrm{solar}} \qquad \text{Eq (1)}$$

where P_{rad} is the thermal radiation power of the cooler, P_{atm} is the power absorbed by the cooler due to incident thermal radiation from the atmosphere, P_{nonrad} accounts for power lost due to conduction and convection, and P_{solar} corresponds to incident absorbed power due to solar irradiation (Bartoli et al. 1977; Nilsson and Niklasson 1995; Zhao et al. 2019). The last term highlights that efficient radiative cooling is more challenging during daytime than during night time due to solar-induced heating when the cooler faces the sky (Bartoli et al. 1977; Nilsson and Niklasson 1995). Daytime radiative coolers therefore need to strongly absorb infrared light (making them strong thermal emitters) while not absorbing light throughout the solar spectrum. Solar radiation must therefore be either transmitted or reflected by the cooling material. Cooling materials that transmit solar radiation are sought for enhancing the performance of solar absorbers

(L. Zhu, Raman, and Fan 2015) and solar cells (L. Zhu et al. 2014), and have been suggested for cooling objects while preserving their color (L. Zhu, Raman, and Fan 2013). For many other applications, it is instead critical that solar radiation is reflected by the cooling material to protect the underlying objects from absorbing and heating up by the sun. Significant effort has been put into creating such reflective radiative coolers, which could cool objects even to sub-ambient temperatures while being exposed to the sun (Rephaeli, Raman, and Fan 2013; Zhai et al. 2017; T. Li et al. 2019; Mandal et al. 2018; Raman et al. 2014; Chen et al. 2016; Zhou et al. 2019; Kou et al. 2017). These reflective radiative coolers prevent solar transmission using back reflectors (Zhai et al. 2017), non-absorbing visible scatterers (L. Zhu, Raman, and Fan 2015) or by micro-porous structures (Mandal et al. 2018; Xiang et al. 2020). They are promising as passive techniques to reduce the need for air-conditioning and refrigeration and thereby have potential to decrease energy consumption devoted to cooling (Goldstein, Raman, and Fan 2017). Hence, there is a need for both transparent and reflective radiative coolers, with ideal systems illustrated in Fig. 1a and 1b, respectively. For transparent coolers we focus on generic systems suitable for different applications, while the transparency window can be further optimized for specific applications, e.g., adopted to the working spectral range of a particular solar cell. Figure 1 shows the ideal reflectance (R), transmittance (T) and absorptance (A) in the UV, visible (VIS) to near IR (NIR) wavelengths and mid-IR (MIR) wavelengths, together with the 1.5 air mass (AM) solar irradiation spectrum (light grey) and the atmospheric IR transparent window (dark grey) from 7 to 14 μm. An ideal transparent radiative cooler (Fig. 1a) is fully transparent (i.e., no reflection or absorption) in the visible spectral range while an ideal reflective cooler instead reflects all visible light (i.e., no transmission or absorption). In the MIR thermal and atmospheric transparency region, both types of materials must possess high absorptance, which via Kirchoff's law of radiation translates to high thermal emissivity and hence, efficient thermal radiation (Greffet et al. 2016).

While the majority of radiative coolers have been based on inorganic materials, organic materials are emerging as promising alternatives. Not least, cellulose and its derivatives have shown promise by providing both high thermal emissivity and low visible absorption (T. Li et al. 2019; Xiang et al. 2020; Gamage et al. 2020). Cellulose is an abundant forest-based material with attractive sustainable properties such as biodegradability, biocompatibility and nontoxicity. Moreover, the nontoxicity and biocompatibility of cellulose-based materials (Wei et al. 2020) make them especially suitable for passive radiative cooler in human body cooling applications (Zhang et al. 2019; Peng et al. 2018; Xiao et al. 2019). Furthermore, the visible properties of cellulose materials can be manipulated by additives or via changes in the structural arrangement at the nanoscale and microscale (Vasileva et al. 2017; Koivurova et al. 2018). For example, highly transparent or translucent materials have been reported based on nanofibrillated cellulose (NFC) (H. Zhu et al. 2013; Fang et al. 2014; Wu et al. 2015; Mahpeykar et al. 2017; Gamage et al. 2020) as well as by delignified and polymer-impregnated wood (Y. Li et al. 2016; Y. Li, Yu, et al. 2017; Y. Li et al. 2018; Y. Li, Fu, et al. 2017). Translucency can be controlled using particle scatterers (Gamage et al. 2020) or by introducing microstructure, which also enables materials to become reflective instead of transparent in the visible range (Xiang et al. 2020). Self-assembly of cellulose nanocrystals into ordered helical structures further allows for materials with structural coloration and preferential reflection of left-hand circularly polarized light (Hewson, Vukusic, and Eichhorn 2017; Fernandes, Lopes, and Godinho 2019).

Our previous work (Gamage et al. 2020) showed that transparent NFC films can be used for sub-ambient daytime radiative cooling. We also embedded silica microparticles as resonant IR absorbers and visible scatterers to control translucency without compromising cooling performance. Such transparent systems are suitable for coatings on solar cells and other optoelectronic devices, but not to cool objects that need protection from solar radiation and corresponding heating. Here, we demonstrate the possibility of creating both reflective and transparent radiative coolers based exclusively on cellulose, without any active additives or back reflectors. The prime difference between the two coolers is the structure of the cellulose at the microscale. The transparent cooler is homogeneous while the reflective cooler is made porous using an

electrospinning process. We characterize the two types of materials in detail using integrating sphere measurements in the UV-VIS-NIR and MIR ranges and we compare them in terms of daytime radiative cooling. We find that the cooling performance is good for both the reflective and transparent cellulose coolers, making them suitable for indoor space cooling and optoelectronics, respectively.

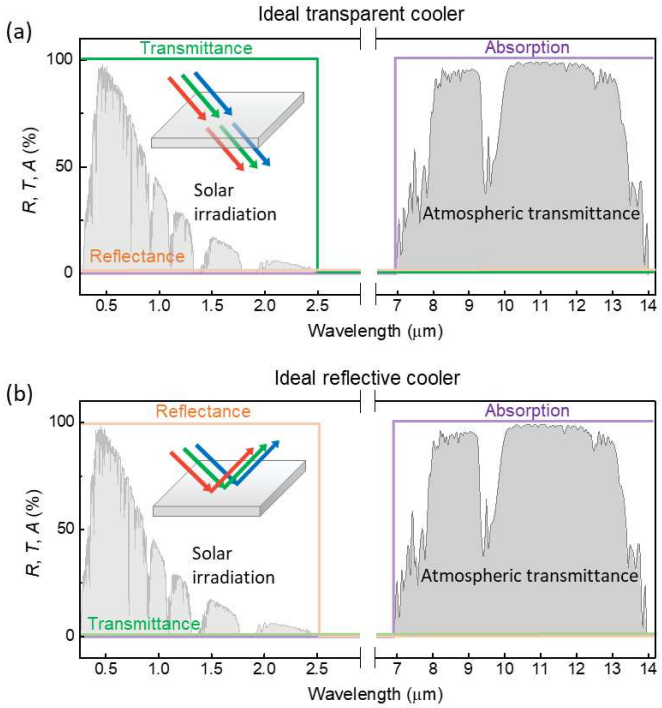

Figure 1. Optical and mid-IR properties of (a) an ideal transparent radiative cooler and (b) an ideal reflective radiative cooler.

Experimental

Materials

Cellulose Acetate, (Mn=30,000), Lithium hydroxide (LiOH), N, N-dimethylformamide (DMF) and Glycerol were purchased from Sigma-Aldrich and used as received. Carboxymethylated NFC was provided by RISE Bioeconomy.

Electrospun cellulose fiber preparation

A solution of 19 weight percentage (wt%) clear cellulose acetate was prepared in co-solvent of DMF and acetone (2:3 volume ratio) under magnetic stirring at room temperature. As depicted in Fig. 2a, the solution was then sucked into a syringe of needle diameter 0.8 mm and fed by a syringe pump with a constant flow rate of 10 µl/min. A high voltage of 25 kV was maintained between the needle and a collector (aluminum foil) separated by 10 cm gap during the electrospinning. The prepared fiber mat was then peeled off from the collector and dipped into aqueous solution of LiOH (0.1 wt %) for 8 h to convert the cellulose acetate to cellulose (see Fig. S1) to obtain a pure cellulose material for suitable comparison with the performance of NFC films. It was then washed 3 times with deionized (DI) water and kept in a fume hood overnight to

dry, resulting in a freestanding porous cellulose fiber mat. We maintained the same electrospinning conditions for all samples presented here and obtained different sample thicknesses by fabrication time.

NFC film casting

The schematic in Fig. 2b demonstrates the NFC film fabrication casting process. A solution of 0.52 wt% NFC in DI water was used for NFC film preparation. In the NFC solution 10% glycerol was added, and the final solution was homogenized for 5 minutes using an ULTRA-TURRAX disperser from IKA Inc. It was then poured into a plastic dish and kept in a drying oven at 40 °C for about 24 hours in order to dry, resulting in a free-standing transparent cellulose film.

Sample characterization

The microstructures of the films were investigated by scanning electron microscopy (SEM), Sigma 500 Gemini from Zeiss AG. Fiber diameter distribution was determined by manual measurements using the line tool of the ImageJ software. For each sample, thickness was measured at 5 different places using a micrometer screw gauge and the average value to the nearest micrometer was taken as the sample thickness.

Reflectance, transmittance and absorptance of samples were determined using spectral directional hemispherical reflectance (DHR) and directional hemispherical transmittance (DHT). Two different spectrometers were used to cover the wavelength regions from the UV to the far IR: A Cary 5000 in the region 250 – 2500 nm and a Bruker Vertex 70 Fourier Transform Infrared (FTIR) spectrometer for the region 2 – 33 µm. Both instruments were equipped with integrating spheres illuminating the sample at an angle of incidence (θ_i) of 8° and 9°, for the Cary and Bruker spectrometers, respectively. A DRA-2500 integrating sphere from Labsphere was used for the Cary spectrophotometer and a Labsphere A562 was used for the Bruker FTIR. The following detectors were used for the different spectral ranges: R928 PMT for UV–VIS, a cooled PbS for NIR up to 2500 nm and a DTGS detector in the IR.

For reflectance measurements, both instruments make use of calibrated reflectance standards (Spectralon® and Infragold® calibrated standards from Labsphere). For the Cary instrument, the reflectance standard was used to collect the baseline, which is used when calculating the sample DHR. The integrating sphere of the Bruker FTIR makes use of an absolute reflection method using the interior wall of the sphere for the baseline measurement, but where the results of the DHR are corrected by a factor obtained from measurements on different calibrated reflectance standards to ensure accurate measurement results. The spectral absorptance is then obtained from the spectral reflectance and transmittance via:

$$R(\lambda) + T(\lambda) + A(\lambda) = 1. \qquad \text{Eq (1)}$$

, with R, T and A being in the range 0 to 1 (or 0% to 100%). We note here that our measurements (DHR and DHT) accounts for diffusive reflection and transmission and not only specular reflection and direct transmission. By Kirchhoff's law of radiation the emissivity at any given wavelength ($\varepsilon(\lambda)$) for a surface in thermal equilibrium is then given by:

$$\varepsilon(\lambda) = A(\lambda) = 1 - T(\lambda) - R(\lambda). \qquad \text{Eq (2)}$$

The value of ε at around 10 µm will determine how efficient a surface at room temperature is at radiating heat, which for a 100% black body radiator is equal 1 (i.e., T and R equal to 0).

Radiative cooling measurements

Figure 4a and 4b show a photograph and a schematic illustration of the radiative cooling measurement setup. Samples were evenly placed in a horizontal plane at the middle of the temperature measurement box of around 40 cm × 30 cm × 15 cm, such that they are equidistant from each other and from the center of the

enclosure. A thin polyethylene (PE) sheet was used to cover the measurement box in order to minimize temperature fluctuations due to wind disturbances. Two thermocouples were used to measure the air temperature inside the box and the average of those two measurements was taken as the ambient temperature. Each cooler was stuck to a Si wafer using stripes of double-sided adhesive tape at the edges to ensure that most of the bottom surface area of the cooler was in direct contact with the Si wafer. Real-time temperature values of the thermocouples were recorded using a LabVIEW program interfaced by an Arduino processor. The radiative cooling measurements were performed in Norrköping, Sweden on May 22, 2020. The maximum outdoor temperature was 16 °C.

1. Results and Discussion

Figure 2a and 2b show the processing and SEM images of cellulose films made by electrospinning and casting, respectively. The two fabrication methods result in highly different structure at the microscale. The electrospun cellulose film is highly porous, composed of a scaffold network of cellulose fibers with micro- and nanoscale dimensions. By contrast, the casted NFC film is highly homogenous. The microporous structure of the electrospun film leads to broadband scattering in the visible region, which makes the film white, in stark contrast to the transparent casted NFC film (see inset photographs in Fig. 2a and 2b). Successful conversion of the cellulose acetate to cellulose was verified *via* changes in the vibrational peaks of FTIR spectra before and after conversion(Huang et al. 2015), as shown in Fig. S1. Examining SEM images for converted cellulose samples indicates a unimodal fiber diameter distribution with a peak around 175 nm.

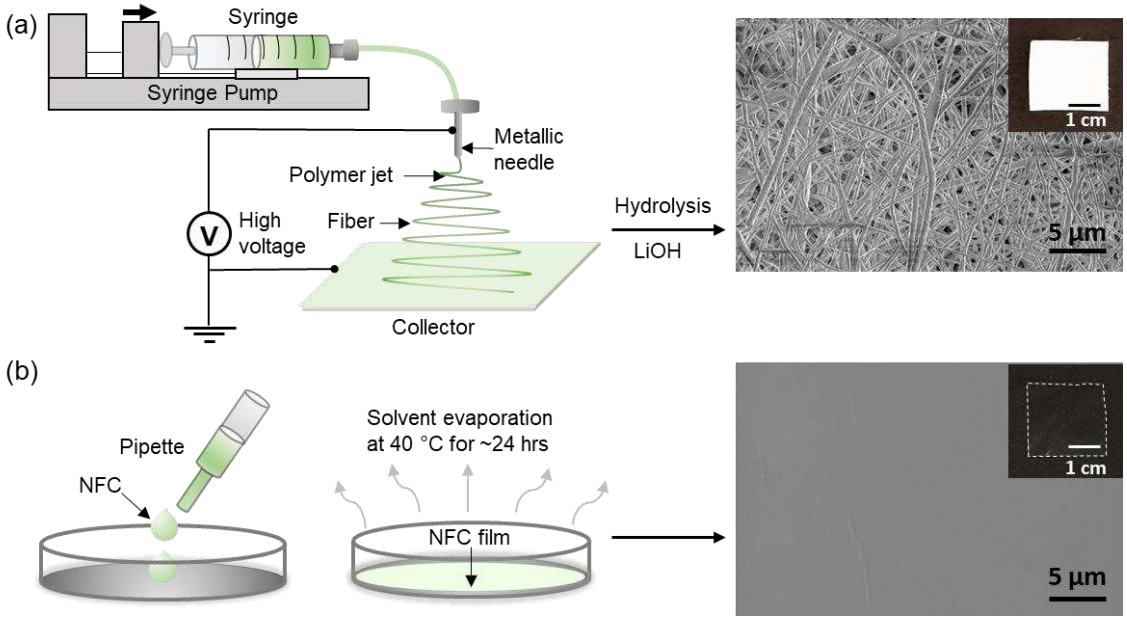

Figure 2. Schematic illustration of process of preparing (a) porous cellulose by electrospinning, and a SEM image of a resulting film and (b) cellulose films by NFC casting, and a SEM image of a resulting homogenous cellulose film. The insets of each SEM image show optical images of the porous cellulose (a) and NFC films (b), respectively. The boundary of NFC film in the optical image is marked with a dashed line as a guide to the eye.

Detailed studies of the reflectance, transmittance and adsorption of the two different cellulose films confirm our initial indications based on visual appearance. As shown in Fig. 3a (blue line), the porous cellulose

material system is exceptionally reflective in the visible, with around 95% reflectance in the range from 0.4 – 0.7 µm for a 275 µm thick sample. The reflectance decreases in the UV but remains above 80% for wavelengths down to 0.25 µm. Likewise, the reflectance slowly decreases but remains fairly high at longer wavelengths all the way to 2.5 µm. The film shows less than 10% transmittance in the whole UV-VIS-NIR region (0.25 – 2.5 µm, Fig. 3b), thereby efficiently preventing light absorption by underlying objects when used as a coating. The broadband high reflection is due to scattering by the wide distribution of nano- and microstructures in the porous material. By contrast, a casted homogenous cellulose film (green line, 65 µm thick) provides high transmittance and less than 10% reflectance in the whole UV-Vis-NIR region (0.25 – 2.5 µm). Based on this marked difference, we now denote the electrospun porous cellulose films as reflective coolers and the homogenous casted films as transparent coolers. Importantly, both types of coolers show almost zero absorption from 0.3 to 1.3 µm (Fig. 3c), which is a promising feature to avoid solar heating of the materials themselves. The absorption increases towards the UV and at longer wavelengths in the NIR, but the solar irradiation is also lower in this range as indicated by the light-grey shaded spectrum. The absorption increases more for the reflective cooler, which we attribute to increased light interaction due to both the microporosity and a higher thickness as compared to the homogenous NFC-based film.

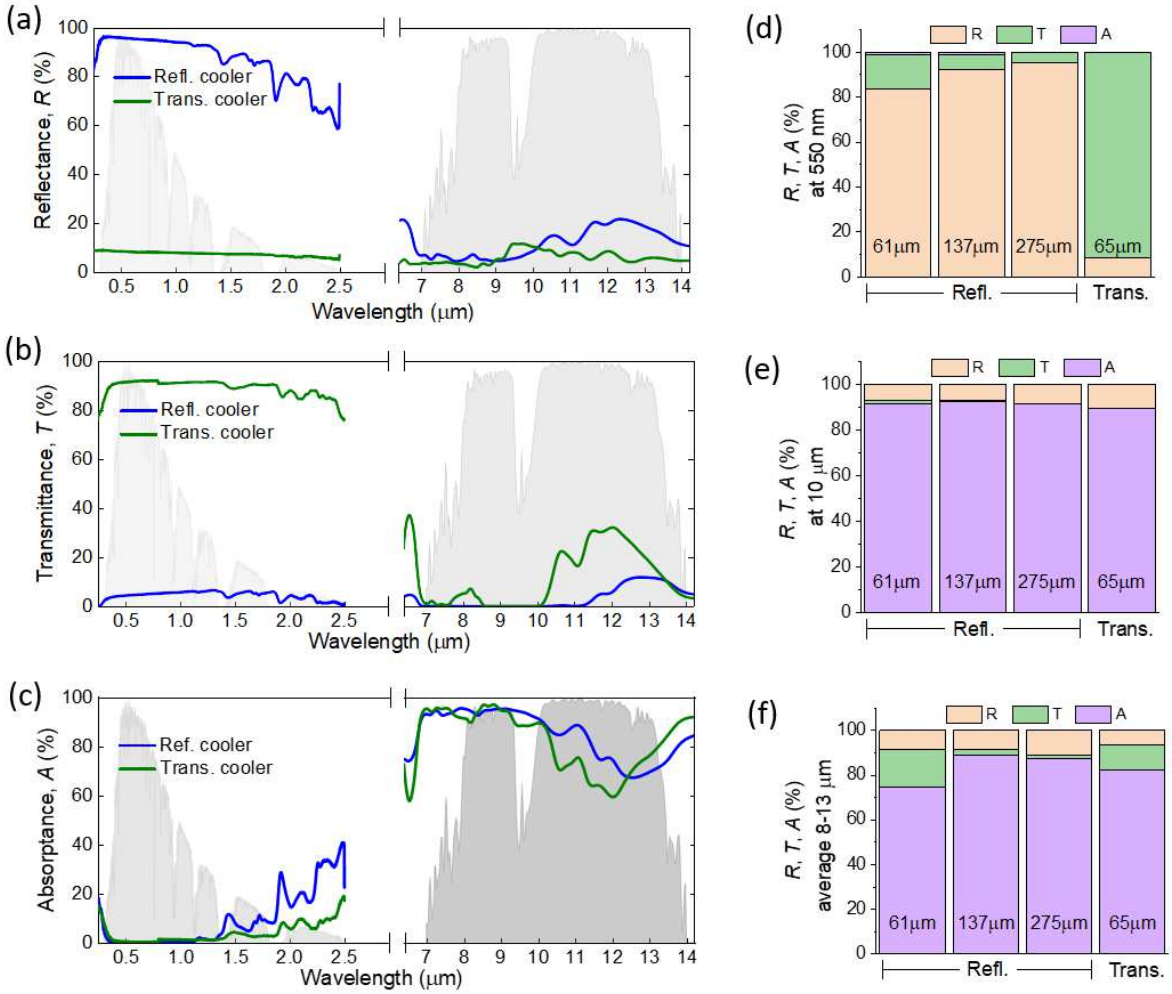

Figure 3. Optical and MIR properties of reflective and transparent coolers. Comparison of (a) reflectance, *R*, (b) transmittance, *T* and (c) absorptance, *A* of a reflective cooler (thickness 275 µm) and a transparent cooler (thickness 65 µm). The grey background spectra in (a-c) correspond to the solar irradiance (light grey) and atmospheric transmittance (dark grey) in arbitrary units. *R*, *T* and *A* of three reflective coolers

(thicknesses 61 μm, 137 μm and 275 μm) and for a 65 μm thick transparent cellulose cooler (d) at 550 nm, (e) at 10 μm and (f) averaged in the range 8-13 μm of the atmospheric transparent window.

While both types of materials show almost zero absorption in the visible, they instead show high absorption in the mid-IR region (Fig. 3c). As discussed above and explained Fig. 1, these combined absorption characteristics makes the materials suitable for daytime passive radiative cooling. From 7 μm to 10 μm, both coolers are almost opaque. The transmission of the reflective cooler further remains low at longer MIR wavelengths while the transparent cooler shows a broad peak at around 12 μm with about 30% transmittance. Comparison between additional samples reveal that this difference in MIR transmittance between the samples is related to differences in film thickness and porosity, as investigated next.

Figure 3d-3f summarizes the visible and MIR properties for three reflective cellulose coolers of different thicknesses (61 μm, 137 μm and 275 μm) and for the 65 μm thick transparent cellulose cooler. Since the visible reflection, transmission and absorption were relatively flat, we present the data at a representative wavelength of 550 nm (Fig. 3d). All three reflective coolers show very low absorption (<3 %) in the visible region. In terms of reflection, even the thinnest reflective cooler provides values higher than 80%. This value increases with thickness, reaching 95% for the thickest reflective cooler. The gradual increase in reflection with thickness can be explained by additional scattering sites for thicker films and corresponding increased probability for light to back scatter instead of escaping the film in the forward direction. Further increasing the electrospun thickness while maintaining film uniformity is challenging because the high voltage applied between needle and collector becomes less effective when more material is deposited on the collector. Fig. 3e presents the equivalent summary of the MIR properties of the same samples. We here used 10 μm as the representative wavelength, at which the thermal emission is peaking at room temperature. We find that all four coolers are essentially opaque at this wavelength, with around 90% absorption and around 10% reflection. Since the MIR atmospheric transparent window spans from about 8 to 13 μm and thermal radiation is spectrally broad, we also present the average MIR properties for the four coolers for this particular region (Fig. 3f). This analysis reveals larger variations between the samples. We first note that the thinnest reflective cooler shows lower absorption (*i.e.,* lower emissivity) and higher transmittance in the MIR compared with the transparent cooler despite very similar thicknesses, which can be explained by lower density and less material in the beam path for the porous material. We further observe that increasing the thickness of the reflective cellulose cooler helps to improve the MIR absorption and thermal emissivity to around 90%. The slightly higher value for the medium thick sample may be due to differences in density resulting from variations in the electrospinning process. The merely 65 μm thick transparent cooler also shows high (>80%) averaged MIR absorption in the atmospheric window, verifying that both types of materials should be suitable for radiative cooling.

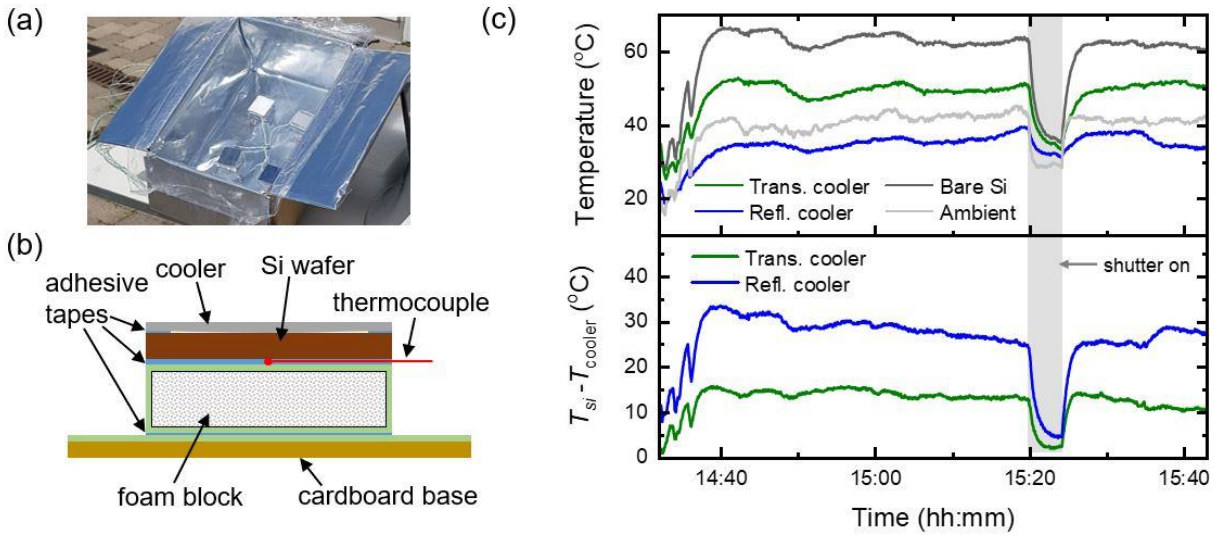

Figure 4. Above ambient cooling performance of transparent and reflective coolers**.** (a) An image of the temperature measurement box with some coolers and bare Si wafer placed in it. (b) Schematic cross-section of a radiative cooler arrangement for measurements with thermocouple and insulating materials. (c) Temperature measurement of two coolers with bare Si wafer during daytime on a sunny day with clear sky. Temperature declination of the two types of coolers relative to temperature of bare Si wafer is given in the bottom of the panel.

From the data presented in Fig. 3, we conclude that both types of cellulose materials possess very low absorption in the visible range while being highly absorptive in the MIR region and thereby efficient thermal emitters. These results suggest that both types of materials are suitable for daytime radiative cooling. We performed real-time outdoor radiative cooling measurements during daytime with reflective and transparent coolers. The sky was clear with no clouds and the relative humidity was in the range of 35-45% throughout the measurements. The coolers were placed in a cardboard box with bottom and side surfaces covered with reflective metalized mylar sheets (see Fig. 4a). Convective heat transfer was minimized using an IR-transparent polyethylene film as wind barrier. We placed foam blocks wrapped with metalized mylar sheets at the bottom of the box and silicon wafers on top of these blocks representing objects to be cooled (and protected from solar heating, see Fig. 4b). The reflective and transparent cellulose radiative coolers were then used as coatings on these Si wafers while monitoring their temperatures during exposure to the sun and the sky. The top panel of Fig. 4c shows the temperature variation during such measurements for Si wafers coated with a reflective cellulose cooler (275 μm thick, blue), a transparent cellulose cooler (65 μm thick, green), a non-coated Si substrate (dark grey) and the ambient temperature in the measurement box (light grey). As soon as the measurement setup was taken outdoor, the temperatures for all components started rising and reached steady-state after a few minutes. The temperature fluctuations during this initial ramping up are due to manual adjustments of the components in the measurement box. At steady state, the temperature of the bare Si wafer reached over 60 °C while the wafers coated with the cellulose coolers both maintained much lower temperatures (around 50 °C and 35°C for the transparent and reflective coolers, respectively). The reduction in temperature (ΔT) by the cellulose coolers are presented in the bottom panel of Fig. 4c. The transparent radiative cooler showed ΔT around 15 °C, despite allowing most of the solar radiation to reach (and heat up) the wafer. This is a significant achievement for a transparent cooler compared to the theoretically suggested value of 18.3 K by Zhu et al (L. Zhu et al. 2014). Similar cooling performance of 14 °C relative to bare Si has been reported for a cooler based on SiO_2 microspheres on glass by Fernandez et al (Jaramillo-Fernandez et al. 2019). The reflective cellulose cooler managed to also prevent

solar-induced heating and reduced the wafer temperature by up to 32 °C. In contrast, Leroy et al (Leroy et al. 2019) reported ΔT of ~ 18 °C during daytime for a polyethylene aerogel based reflective cooler during below ambient cooling measurements. Excitingly, the reflective cooler continuously managed to maintain temperatures even several degrees Celsius below the ambient air temperature inside the box. Such sub-ambient daytime cooling highlights the dual ability of the reflective cooler to both prevent objects from solar heating and to efficiently remove heat by radiative cooling. At 15:20 we covered the whole setup with a shutter for a few minutes (shaded region in Fig. 4c), blocking exposure to the sky. During this period, the ambient temperature became lowest and when the shutter opened again, all objects again reached their previous temperatures within a few minutes. Figure S3 shows a similar experiment performed without IR transparent wind barrier. Also here, both coolers could reduce the temperature of the underlying Si wafers compared with the non-coated Si. Again, the reflective cooler was most effective, reducing the temperature by up to 15 °C to achieve similar values as the ambient temperature in the box. The overall lower absolute temperatures for all samples when not using the wind barrier (also for the non-coated Si sample) is attributed to additional convective heat removal and less green-house effects. The optical properties of Si wafer used as substrate are given in Fig. S4.

Conclusion

Our study shows that cellulose is suitable for passive radiative cooling and that different types of coolers can be made by varying the material preparation method. We used this principle to form homogenous films by casting and porous fiber network films by electrospinning. Even though both of these materials are cellulose-based, they demonstrate totally opposite visible reflection/transmission due their structural differences at the nano- and microscales. They both further show very low solar absorption combined with high thermal emissivity in the MIR. The average IR absorption, and hence emissivity, of both materials is greater than 70% for all investigated sample thicknesses and reached up to 90% emissivity at 10 μm that corresponds to thermal emission at room temperature. Daytime radiative cooling measurements demonstrate that the reflective and transparent coolers could reduce the temperature of coated silicon wafers by around 30 °C and 15 °C, respectively. Moreover, the reflective cooler reached a few degrees even below the ambient temperature. These results suggest that transparent cellulose may be used as coating material for optoelectronic and solar harvesting devices to overcome the heat-induced efficiency drops, while reflective cellulose shows promise for cooling heat loads underneath, such as water masses for building space cooling systems.

Acknowledgements

The authors acknowledge financial support from the Knut and Allice Wallenberg Foundation via a Wallenberg Scholarship; the Knut and Alice Wallenberg foundation, Linköping University and industry through the Wallenberg Wood Science Center; the Swedish Government Strategic Research Area in Materials Science on Functional Materials at Linköping University (Faculty Grant SFO-Mat-LiU No. 2009 00971), the Swedish Foundation for Strategic Research and the Swedish Armed Forces Research and Technology program and the Swedish Research Council (VR 2016-06146). The authors also thank Meysam Karami Rad for help with constructing the temperature measurement setup, and Ravi Shanker for assistance with plotting solar irradiation and atmospheric transmittance spectra.

Compliance with ethical standards

Conflicts of interest The authors have no conflict of interests.

Ethical approval The study was completed by following ethical standards.

References

Bartoli, B., S. Catalanotti, B. Coluzzi, V. Cuomo, V. Silvestrini, and G. Troise. 1977. "Nocturnal and Diurnal Performances of Selective Radiators." *Applied Energy*. https://doi.org/10.1016/0306-2619(77)90015-0.

Chen, Zhen, Linxiao Zhu, Aaswath Raman, and Shanhui Fan. 2016. "Radiative Cooling to Deep Sub-Freezing Temperatures through a 24-h Day-Night Cycle." *Nature Communications*. https://doi.org/10.1038/ncomms13729.

Fang, Zhiqiang, Hongli Zhu, Yongbo Yuan, Dongheon Ha, Shuze Zhu, Colin Preston, Qingxia Chen, et al. 2014. "Novel Nanostructured Paper with Ultrahigh Transparency and Ultrahigh Haze for Solar Cells." *Nano Letters*. https://doi.org/10.1021/nl404101p.

Fernandes, S. N., L. F. Lopes, and M. H. Godinho. 2019. "Recent Advances in the Manipulation of Circularly Polarised Light with Cellulose Nanocrystal Films." *Current Opinion in Solid State and Materials Science*. https://doi.org/10.1016/j.cossms.2018.11.004.

Gamage, Sampath, Evan S.H. Kang, Christina Åkerlind, Samim Sardar, Jesper Edberg, Hans Kariis, Thomas Ederth, Magnus Berggren, and Magnus P. Jonsson. 2020. "Transparent Nanocellulose Metamaterial Enables Controlled Optical Diffusion and Radiative Cooling." *Journal of Materials Chemistry C*. https://doi.org/10.1039/d0tc01226b.

Goldstein, Eli A., Aaswath P. Raman, and Shanhui Fan. 2017. "Sub-Ambient Non-Evaporative Fluid Cooling with the Sky." *Nature Energy*. https://doi.org/10.1038/nenergy.2017.143.

Greffet, Jean-Jacques, Patrick Bouchon, Giovanni Brucoli, Emilie Sakat, and François Marquier. 2016. "Generalized Kirchhoff Law," January. https://doi.org/10.1103/PhysRevX.8.021008.

Hewson, D., P. Vukusic, and S. J. Eichhorn. 2017. "Reflection of Circularly Polarized Light and the Effect of Particle Distribution on Circular Dichroism in Evaporation Induced Self-Assembled Cellulose Nanocrystal Thin Films." *AIP Advances*. https://doi.org/10.1063/1.4986761.

Huang, Fenglin, Yunfei Xu, Bin Peng, Yangfen Su, Feng Jiang, You Lo Hsieh, and Qufu Wei. 2015. "Coaxial Electrospun Cellulose-Core Fluoropolymer-Shell Fibrous Membrane from Recycled Cigarette Filter as Separator for High Performance Lithium-Ion Battery." *ACS Sustainable Chemistry and Engineering*. https://doi.org/10.1021/acssuschemeng.5b00032.

Jaramillo-Fernandez, Juliana, Guy L. Whitworth, Jose Angel Pariente, Alvaro Blanco, Pedro D. Garcia, Cefe Lopez, and Clivia M. Sotomayor-Torres. 2019. "A Self-Assembled 2D Thermofunctional Material for Radiative Cooling." *Small*. https://doi.org/10.1002/smll.201905290.

Koivurova, Matias, Elena Vasileva, Yuanyuan Li, Lars Berglund, and Sergei Popov. 2018. "Complete Spatial Coherence Characterization of Quasi-Random Laser Emission from Dye Doped Transparent Wood." *Optics Express*. https://doi.org/10.1364/oe.26.013474.

Kou, Jun long, Zoila Jurado, Zhen Chen, Shanhui Fan, and Austin J. Minnich. 2017. "Daytime Radiative Cooling Using Near-Black Infrared Emitters." *ACS Photonics*. https://doi.org/10.1021/acsphotonics.6b00991.

Leroy, A., B. Bhatia, C. C. Kelsall, A. Castillejo-Cuberos, M. H. Di Capua, L. Zhao, L. Zhang, A. M. Guzman, and E. N. Wang. 2019. "MATERIALS SCIENCE High-Performance Subambient Radiative Cooling Enabled by Optically Selective and Thermally Insulating Polyethylene Aerogel." *Science Advances*. https://doi.org/10.1126/sciadv.aat9480.

Li, Tian, Yao Zhai, Shuaiming He, Wentao Gan, Zhiyuan Wei, Mohammad Heidarinejad, Daniel Dalgo, et al. 2019. “A Radiative Cooling Structural Material.” *Science (New York, N.Y.)*. https://doi.org/10.1126/science.aau9101.

Li, Yuanyuan, Qiliang Fu, Ramiro Rojas, Min Yan, Martin Lawoko, and Lars Berglund. 2017. “Lignin-Retaining Transparent Wood.” *ChemSusChem*. https://doi.org/10.1002/cssc.201701089.

Li, Yuanyuan, Qiliang Fu, Xuan Yang, and Lars Berglund. 2018. “Transparent Wood for Functional and Structural Applications.” *Philosophical Transactions of the Royal Society A: Mathematical, Physical and Engineering Sciences*. https://doi.org/10.1098/rsta.2017.0182.

Li, Yuanyuan, Qiliang Fu, Shun Yu, Min Yan, and Lars Berglund. 2016. “Optically Transparent Wood from a Nanoporous Cellulosic Template: Combining Functional and Structural Performance.” *Biomacromolecules*. https://doi.org/10.1021/acs.biomac.6b00145.

Li, Yuanyuan, Shun Yu, Jonathan G.C. Veinot, Jan Linnros, Lars Berglund, and Ilya Sychugov. 2017. “Luminescent Transparent Wood.” *Advanced Optical Materials*. https://doi.org/10.1002/adom.201600834.

Mahpeykar, S M, Y B Zhao, X Y Li, Z Y Yang, Q W Xu, Z H Lu, E H Sargent, and X H Wang. 2017. “Cellulose Nanocrystal:Polymer Hybrid Optical Diffusers for Index-Matching-Free Light Management in Optoelectronic Devices.” *Advanced Optical Materials* 5 (21). https://doi.org/ARTN 170043010.1002/adom.201700430.

Mandal, Jyotirmoy, Yanke Fu, Adam C. Overvig, Mingxin Jia, Kerui Sun, Norman N. Shi, Hua Zhou, Xianghui Xiao, Nanfang Yu, and Yuan Yang. 2018. “Hierarchically Porous Polymer Coatings for Highly Efficient Passive Daytime Radiative Cooling.” *Science*. https://doi.org/10.1126/science.aat9513.

Nilsson, Torbjörn M.J., and Gunnar A. Niklasson. 1995. “Radiative Cooling during the Day: Simulations and Experiments on Pigmented Polyethylene Cover Foils.” *Solar Energy Materials and Solar Cells*. https://doi.org/10.1016/0927-0248(94)00200-2.

Peng, Yucan, Jun Chen, Alex Y. Song, Peter B. Catrysse, Po Chun Hsu, Lili Cai, Bofei Liu, et al. 2018. “Nanoporous Polyethylene Microfibres for Large-Scale Radiative Cooling Fabric.” *Nature Sustainability*. https://doi.org/10.1038/s41893-018-0023-2.

Raman, A P, M A Anoma, L Zhu, E Rephaeli, and S Fan. 2014. “Passive Radiative Cooling below Ambient Air Temperature under Direct Sunlight.” *Nature* 515 (7528): 540–44. https://doi.org/10.1038/nature13883.

Rephaeli, Eden, Aaswath Raman, and Shanhui Fan. 2013. “Ultrabroadband Photonic Structures to Achieve High-Performance Daytime Radiative Cooling.” *Nano Letters*. https://doi.org/10.1021/nl4004283.

Vasileva, Elena, Yuanyuan Li, Ilya Sychugov, Mounir Mensi, Lars Berglund, and Sergei Popov. 2017. “Lasing from Organic Dye Molecules Embedded in Transparent Wood.” *Advanced Optical Materials*. https://doi.org/10.1002/adom.201700057.

Wei, Wei, Yong Zhu, Qiu Li, Zefeng Cheng, Yongji Yao, Qi Zhao, Pan Zhang, et al. 2020. “An Al2O3-Cellulose Acetate-Coated Textile for Human Body Cooling.” *Solar Energy Materials and Solar Cells*. https://doi.org/10.1016/j.solmat.2020.110525.

Wu, W, N G Tassi, H L Zhu, Z Q Fang, and L B Hu. 2015. “Nanocellulose-Based Translucent Diffuser for Optoelectronic Device Applications with Dramatic Improvement of Light Coupling.” *Acs Applied Materials & Interfaces* 7 (48): 26860–64. https://doi.org/10.1021/acsami.5b09249.

Xiang, Bo, Rong Zhang, Yanlong Luo, Sheng Zhang, Lei Xu, Huihua Min, Shaochun Tang, and Xiangkang Meng. 2020. "3D Porous Polymer Film with Designed Pore Architecture and Auto-Deposited SiO2 for Highly Efficient Passive Radiative Cooling." *Nano Energy*, 105600. https://doi.org/https://doi.org/10.1016/j.nanoen.2020.105600.

Xiao, Runcai, Chengyi Hou, Weifeng Yang, Yun Su, Yaogang Li, Qinghong Zhang, Peng Gao, and Hongzhi Wang. 2019. "Infrared-Radiation-Enhanced Nanofiber Membrane for Sky Radiative Cooling of the Human Body." *ACS Applied Materials and Interfaces*. https://doi.org/10.1021/acsami.9b13933.

Zhai, Yao, Yaoguang Ma, Sabrina N. David, Dongliang Zhao, Runnan Lou, Gang Tan, Ronggui Yang, and Xiaobo Yin. 2017. "Scalable-Manufactured Randomized Glass-Polymer Hybrid Metamaterial for Daytime Radiative Cooling." *Science* 355 (6329): 1062–66. https://doi.org/10.1126/science.aai7899.

Zhang, Xu A., Shangjie Yu, Beibei Xu, Min Li, Zhiwei Peng, Yongxin Wang, Shunliu Deng, et al. 2019. "Dynamic Gating of Infrared Radiation in a Textile." *Science*. https://doi.org/10.1126/science.aau1217.

Zhao, Dongliang, Ablimit Aili, Yao Zhai, Shaoyu Xu, Gang Tan, Xiaobo Yin, and Ronggui Yang. 2019. "Radiative Sky Cooling: Fundamental Principles, Materials, and Applications." *Applied Physics Reviews*. https://doi.org/10.1063/1.5087281.

Zhou, Lyu, Haomin Song, Jianwei Liang, Matthew Singer, Ming Zhou, Edgars Stegenburgs, Nan Zhang, et al. 2019. "A Polydimethylsiloxane-Coated Metal Structure for All-Day Radiative Cooling." *Nature Sustainability*. https://doi.org/10.1038/s41893-019-0348-5.

Zhu, Hongli, Sepideh Parvinian, Colin Preston, Oeyvind Vaaland, Zhichao Ruan, and Liangbing Hu. 2013. "Transparent Nanopaper with Tailored Optical Properties." *Nanoscale*. https://doi.org/10.1039/c3nr00520h.

Zhu, Linxiao, Aaswath Raman, and Shanhui Fan. 2013. "Color-Preserving Daytime Radiative Cooling." *Applied Physics Letters*. https://doi.org/10.1063/1.4835995.

Zhu, Linxiao, Aaswath P. Raman, and Shanhui Fan. 2015. "Radiative Cooling of Solar Absorbers Using a Visibly Transparent Photonic Crystal Thermal Blackbody." *Proceedings of the National Academy of Sciences of the United States of America*. https://doi.org/10.1073/pnas.1509453112.

Zhu, Linxiao, Aaswath Raman, Ken Xingze Wang, Marc Abou Anoma, and Shanhui Fan. 2014. "Radiative Cooling of Solar Cells." *Optica*. https://doi.org/10.1364/optica.1.000032.

Figures

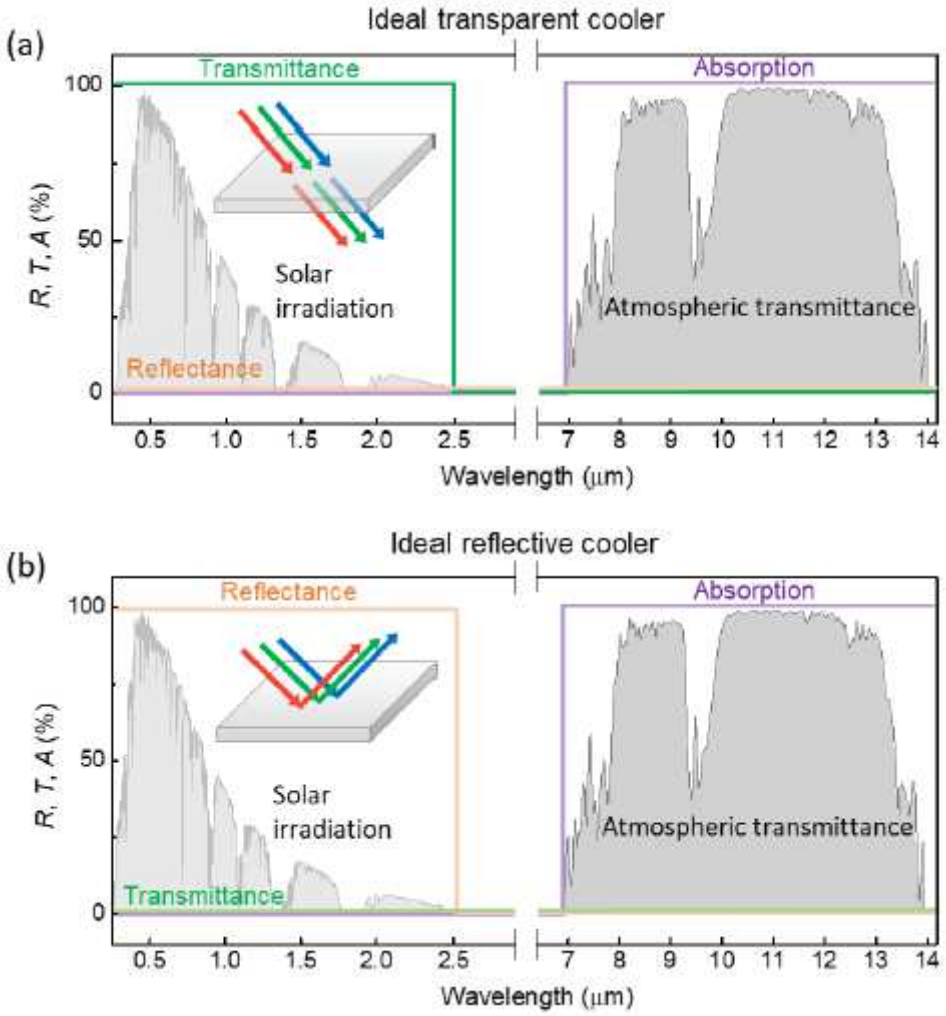

Figure 1

Optical and mid-IR properties of (a) an ideal transparent radiative cooler and (b) an ideal reflective radiative cooler.

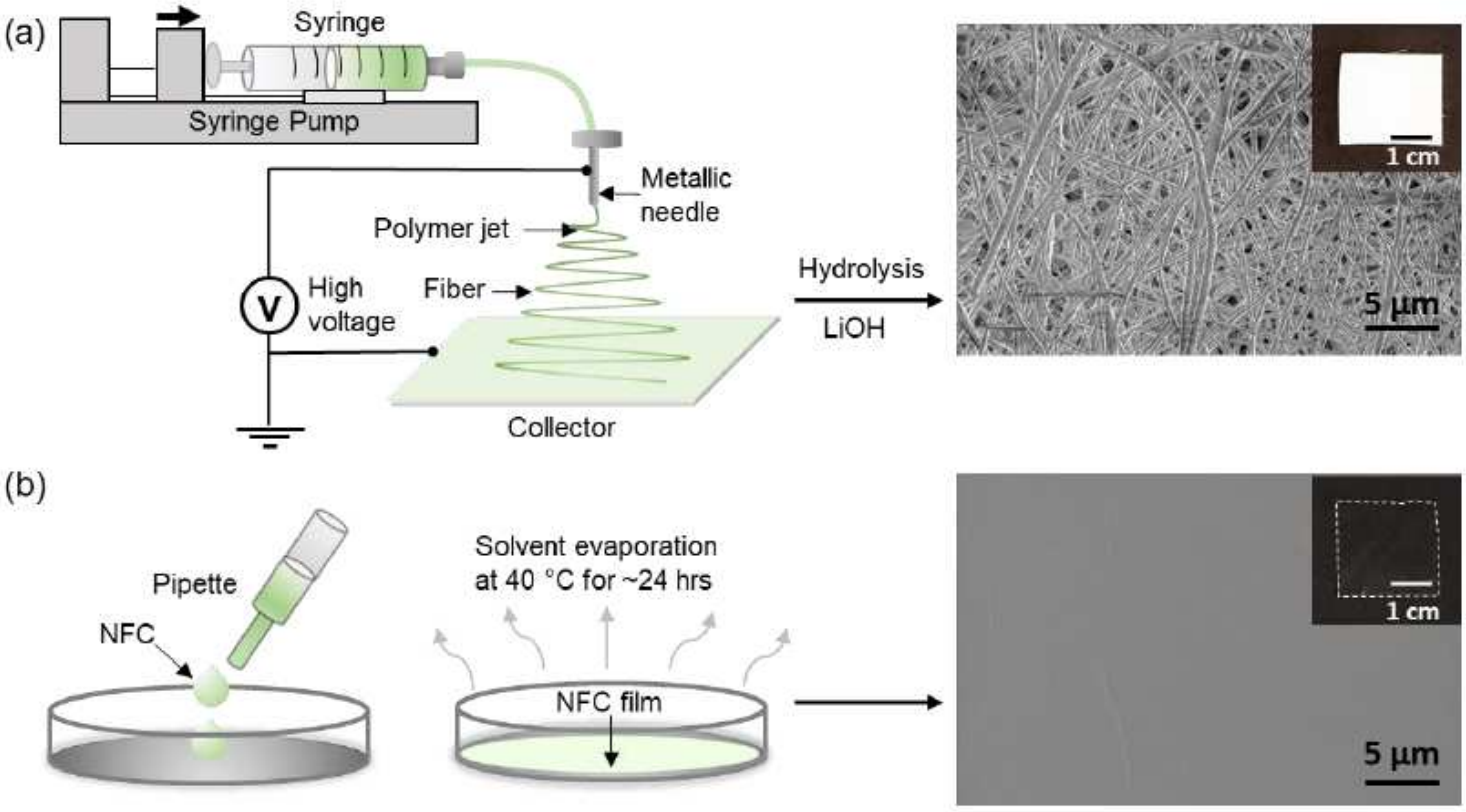

Figure 2

Schematic illustration of process of preparing (a) porous cellulose by electrospinning, and a SEM image of a resulting film and (b) cellulose films by NFC casting, and a SEM image of a resulting homogenous cellulose film. The insets of each SEM image show optical images of the porous cellulose (a) and NFC films (b), respectively. The boundary of NFC film in the optical image is marked with a dashed line as a guide to the eye.

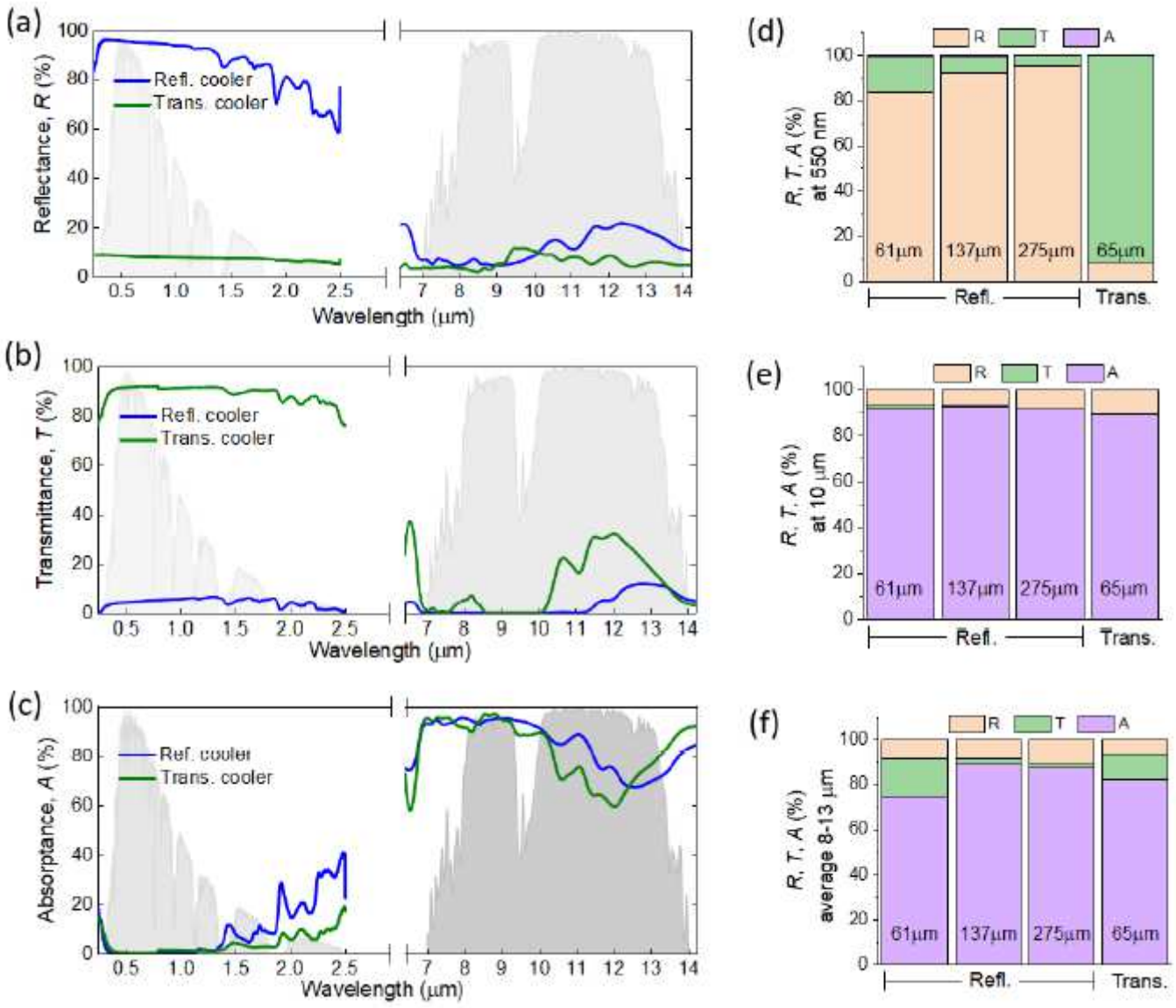

Figure 3

Optical and MIR properties of reflective and transparent coolers. Comparison of (a) reflectance, R, (b) transmittance, T and (c) absorptance, A of a reflective cooler (thickness 275 μm) and a transparent cooler (thickness 65 μm). The grey background spectra in (a-c) correspond to the solar irradiance (light grey) and atmospheric transmittance (dark grey) in arbitrary units. R, T and A of three reflective coolers (thicknesses 61 μm, 137 μm and 275 μm) and for a 65 μm thick transparent cellulose cooler (d) at 550 nm, (e) at 10 μm and (f) averaged in the range 8-13 μm of the atmospheric transparent window.

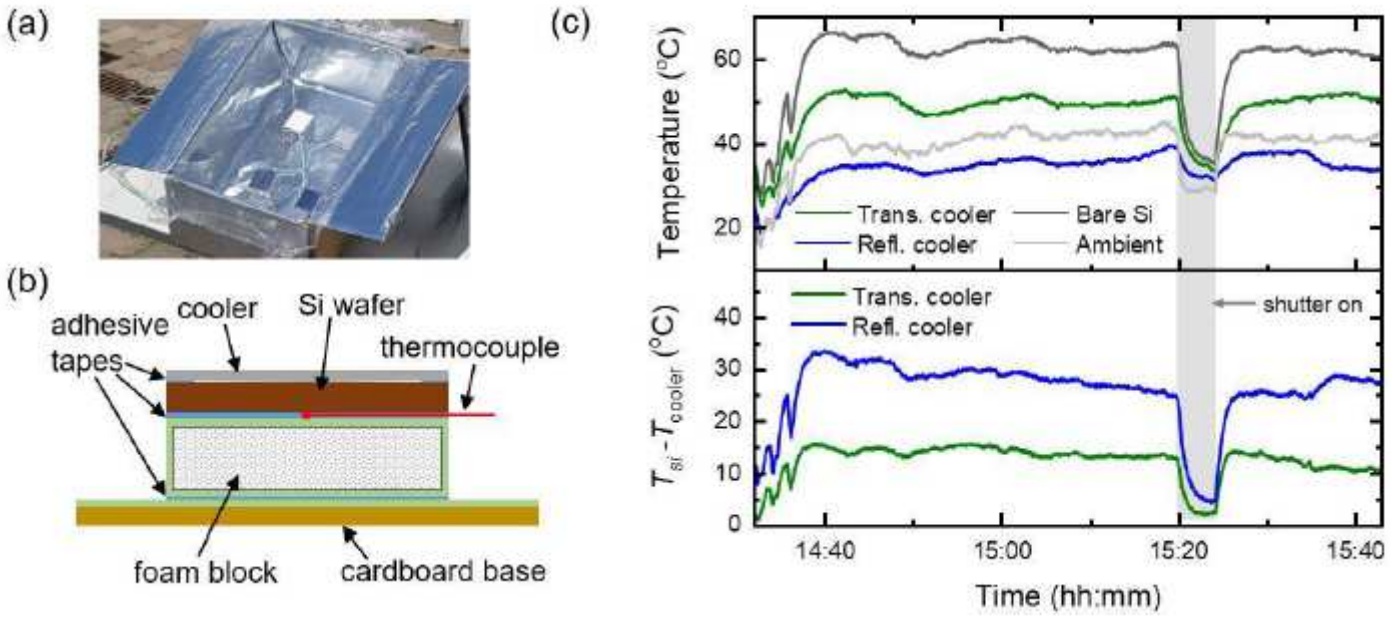

Figure 4

Above ambient cooling performance of transparent and reflective coolers. (a) An image of the temperature measurement box with some coolers and bare Si wafer placed in it. (b) Schematic cross-section of a radiative cooler arrangement for measurements with thermocouple and insulating materials. (c) Temperature measurement of two coolers with bare Si wafer during daytime on a sunny day with clear sky. Temperature declination of the two types of coolers relative to temperature of bare Si wafer is given in the bottom of the panel.

Supplementary Files

This is a list of supplementary files associated with this preprint. Click to download.

- 20210305Electronicsupplementarymaterial.pdf